R&D NOTES

An Eulerian/Lagrangian Study of Solid Suspension in Stirred Tanks

T. Srinivasa and S. Jayanti
Dept. of Chemical Engineering, IIT Madras, Chennai 600036, India

DOI 10.1002/aic.11253
Published online July 20, 2007 in Wiley InterScience (www.interscience.wiley.com).

Keywords: solid suspension, stirred tanks, critical suspension, computational fluid dynamics, particle tracking, turbulent dispersion

Introduction

Mixing and solid suspension are important unit operations in many chemical, pharmaceutical, cosmetics, polymer, and other process industries. Solid suspension is often effected by a stirred vessel, in which one or more impellers rotate at a constant rotational speed; the resulting liquid flow entrains the particles and keeps them suspended. In these vessels it is important that solid particles, which may act as a catalyst or may undergo reaction, are completely suspended to ensure that the maximum surface area is available; a perfect homogenization at further expenditure of energy may not be desirable. Thus, the critical suspension speed, N_{cs}, which is the rotational speed of the impeller at which the particles are just suspended, becomes an important design parameter.

There is a close interplay between the suspension of particles and the flow field generated by the impeller. The flow pattern in a stirred vessel is often complicated, three-dimensional, recirculating, turbulent, and is sensitive to geometrical features of the impeller as well as those of the vessel. The suspension of the particles is in addition affected by factors such as the particle density, size, shape, density of loading, etc. A number of geometric parameters of the impeller are considered during the design of an impeller for a given suspension duty. These include the diameter and height of the tank, the type, diameter, height, width, pitch, and number of the blades. There have been a number of mostly experimental studies of suspension and empirical criteria have been evolved over the past several decades for the design and for determining the critical impeller speed of impellers.[1–6] A large amount of literature dealing with solid suspension using different types of impellers is available. Books and reviews on mixing and solids suspension include those of Nagata,[7] Harnby et al.,[8] and Tatterson.[9]

There is a trend in recent years to design impellers using computational fluid dynamics (CFD)-based simulations. Here the problem is approached by solving the fundamental fluid flow equations, such as the conservation of mass and conservation of momentum, for the fluid stirred by the impeller. The equations can be solved numerically using industrial scale geometry; hence uncertainties in scaling-up or down are eliminated. Advances in modeling of rotating systems allow the computation of the flow field created by multiple impellers of different types mounted on the same shaft and rotating at different speeds. CFD simulations also enable one to take proper account of the presence of internal parts, such as detection probes, thermocouple wells, internal coils, etc., and the location of these inside the vessel, which are known to affect the critical suspension speed. Rewatkar et al.[4] reported that even the presence of gas sparger increased the critical impeller speed for a solid suspension. It is possible to take account of the effect of these on the hydrodynamics in a CFD-based calculation.

The treatment of solids in these two-phase (gas–liquid) calculations falls into one of two broad categories of approaches, namely, the Eulerian/Eulerian and the Eulerian/Lagrangian approaches. In the former, the two phases are considered to be interpenetrating continua and field equations representing the conservation of mass and momentum are solved for both the phases. In this approach, the dynamics of multiphase systems is captured through the modeling of the phase interaction terms that appear in the conservation equations. In the Eulerian/Lagrangian approach, the conventional field equations are used to solve the flow field of the continuous phase, and the dispersed phase is brought into analysis by tracking representative particles as they move through the flow domain. The interphase interaction is evaluated in terms of source/sink terms, which arise along the path of the par-

Correspondence concerning this article should be addressed to S. Jayanti at sjayanti@iitm.ac.in.

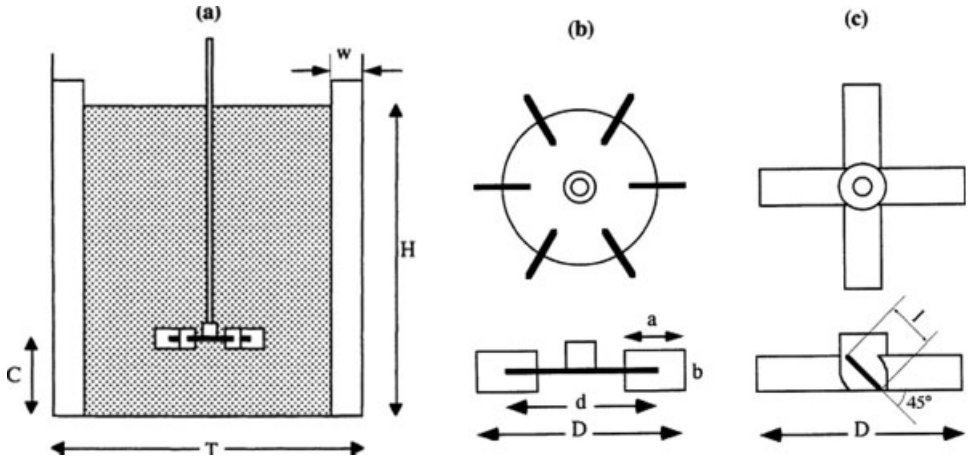

Figure 1. Details of the tank-mixer system: (a) standard baffled vessel, (b) a disk turbine impeller, and (c) a pitched blade impeller.

ticles, in the conservation equations for the continuous phase. In spite of the conceptual simplicity of this approach, much of the work on CFD simulation of solid dispersion in agitated vessels has been done using the Eulerian/Eulerian approach[10–14] as the solution of the field equations is relatively straightforward. However, the results of these calculations cannot be interpreted in an unambiguous way, and it has not been possible to develop a clear criterion for the critical speed using this approach. In contrast, particle tracking allows one to determine whether or not a particle of given characteristics (size, density) is entrained by a given flow field. The objective of the present work is to explore the possibility of using this as a basis to determine the condition of critical suspension. To this end, a number of the Eulerian/Lagrangian approach-based CFD simulations have been done under various conditions. A physically-appealing and numerically implementable criterion for the critical impeller speed has been established and it is shown that it gives qualitatively correct results with a number of experimental observations. Details of the calculations and the results are discussed later.

Details of the Calculations

Geometry

The stirred tank has a standard configuration as shown in Figure 1a. It consists of a cylindrical flat-bottomed, baffled open tank with diameter (T) equal to the liquid height (H). Various types of impellers are used in mixing and solid suspending operations. Based on the type of the flow they generate, they can be classified as radial and axial flow impellers. In the present work, three impellers (Figures 1b, c) are considered: the disk turbine (DT) which generates mainly radial flow, and two configurations of the pitched blade turbine, namely, the pitched blade turbine with down flow (PTD) and the pitched blade turbine with up flow (PTU). Three diameters of the impeller (D) have been considered for the same tank diameter ($T/D = 2$, 3, and 4). Other geometrical details are summarized in Table 1; these correspond to standard stirrer configurations.[3,4,15] The fluid (water) and the solid (sand) were kept the same in all calculations and the effect of impeller diameter, type of impeller and rotational speed and particle size for fixed tank diameter and off-bottom clearance for the sand-water system has been studied. Additional calculations have been done with particles of silica and calcium sulphate to investigate the effect of particle density on the critical suspension speed.

Flow field

The flow field and the particle trajectory calculations have been carried out using the commercial CFD codes MIXSIM-2 and FLUENT-6.2 developed by Fluent, USA. The MIXSIM was used to create the geometry and to generate the grid and the FLUENT was used to obtain the flow field and the particle trajectories. The nature of the continuous phase flow calculations is similar to that done, among others, by Shekhar and Jayanti.[16] The flow in mixing tanks of low viscosity liquids (as in the present case) is expected to be turbulent; the usual practice of using the Reynolds-averaged form of Navier-Stokes (RANS) equations along with a turbulence model, the k–ε model in the present case, was used to obtain the turbulent flow field. The rotation of the impeller poses

Table 1. Geometrical Parameters of Standard Stirrer Configuration[15]

Parameter	Value
Tank diameter, T	T
Impeller diameter, D	$T/D = 2$, 3, or 4
Bottom clearance, C	$T/C = 2$, 3, or 4
Liquid height, H	$T/H = 1$
Width of the baffles, w	$T/10$
Length of the blade, a	$D/4$
Height of the blade, b	$D/5$
Shaft diameter, d_s	$0.12D$
Diameter of the disk, d	$^3/_4D$
Blade thickness, b_t	$0.12D$
Number of blades	6
Pitch angle (for PTD and PTU)	45°
Impeller speed, rpm	360–1000

special problems in calculating the continuous phase flow field because of the presence of a moving boundary in a fixed mesh. A number of alternatives are available in such cases.[17] If the impeller–baffle interaction is weak, then the steady-state formulation of the multiple reference frame (MRF) approach can be used. Here, the individual cell zones are assumed to move at different rotational/translational speeds and the flow at the boundaries between these zones is assumed to be nearly aligned. While the MRF approach is clearly an approximation, it can provide a reasonable model of the time-averaged flow in the present case since the impeller–baffle gap is quite large and, by design, large-scale transient effects associated with baffles are not present.

Particle motion

The trajectory of a discrete phase particle is obtained by integrating the momentum balance on the particle in a Lagrangian reference frame:

$$m_{\mathrm{p}} \frac{du_{\mathrm{p}}}{dt} = \sum F_{\mathrm{ext}} \tag{1}$$

Here, m_{p} is the particle mass, u_{p} is its velocity, and F_{ext} are the external forces acting on it; the buoyancy force due to gravity, the added (virtual) mass force due to relative acceleration of the particulate phase and the viscous drag force of the fluid are included in the analysis. While the calculation of the buoyancy force is straightforward, the added mass force is calculated using a constant added mass coefficient of 0.5 (applicable for spherical particles), and the drag force is calculated using a Reynolds number-dependent drag coefficient correlation, which closely mimics the standard drag curve for a spherical particle over Stokes, intermediate, and inertial regions. The particle displacement is calculated using forward Euler integration of the particle velocity over time step, δt

$$x_i^n = x_i^o + u_{\mathrm{pi}} \delta t \tag{2}$$

where the superscripts o and n refer to old and new values, respectively, and u_{pi} is the particle velocity. The particle velocity calculated at the start of the time step is assumed to prevail over the entire step and a new particle velocity is calculated at the end of the time step using Eq. 1. The application of Lagrangian tracing involves the integration of particle paths through the discretized domain. Individual particles are tracked from their injection point until they escape the domain or some integration limit criterion is met. Each representative particle is tracked to generate a particle path along which source terms to the fluid mass, momentum and energy equations are computed which represent the particle-fluid interaction along the path. Because each particle is tracked from its injection point to final destination, the tracking procedure is applicable to (quasi-) steady state flow analysis. Also, particle–particle interaction cannot be taken into account as each representative particle is tracked individually. This limits the approach to dilute suspensions only.

When the flow is turbulent, and the particles are small, the particle motion can be significantly affected by the turbulence. The dispersion of particles due to turbulence in the fluid phase is predicted using a stochastic tracking method based on the model of Hutchinson et al.[18] This model includes the effect of instantaneous turbulent velocity fluctuations on the particle trajectories. Each particle is assumed to encounter a series of turbulent eddies of random size, strength and orientation as it passes through the flow domain and a particle is assumed to be always within a single eddy. Each eddy has a characteristic fluctuating velocity u_{f}', a life time, τ_{e}, and a length, l_{e}. When a particle enters an eddy, the fluctuating velocity for that eddy is added to the local mean fluid velocity to obtain the instantaneous fluid velocity, which is then used in calculating the drag and other forces acting on the particle. The addition of the fluctuating velocity component of random orientation to the mean velocity enables transverse motion of particles even in a steady, one-dimensional mean velocity field. The turbulent fluid velocity, u_{f}', is assumed to prevail as long as the particle/eddy interaction time is less than the eddy life time and the displacement of the particle relative to the eddy is less than the eddy length. If either of these conditions is exceeded, the particle is assumed to enter a new eddy with a new characteristic u_{f}', τ_{e}, and l_{e}. The characteristic fluctuating velocity, eddy life time and length are calculated based on the local turbulence properties of the flow:

$$l_{\mathrm{e}} = \frac{C_\mu^{3/4} k^{3/2}}{\varepsilon} \tag{3}$$

$$u_{\mathrm{f}}' = \Gamma \left(\frac{2k}{3}\right)^{0.5} \tag{4}$$

$$\tau_{\mathrm{e}} = \frac{l_{\mathrm{e}}}{\left(2k/3\right)^{1/2}} \tag{5}$$

where k and ε are local turbulent kinetic energy and dissipation, respectively, C_μ is a modeling constant having a value of 0.09, and Γ is a normally distributed random number. Thus, this model represents the effect of the so-called energy containing eddies (the size of which is expected to be large when compared with that of the particles) of the turbulence spectrum on the particles. The effect of small size eddies (in the intermediate and Kolmogorov wave number range) is not considered. Given that one is interested in the just-suspended criterion (and not the homogenization) in an impeller-generated turbulent flow field, taking account of role of just the largest turbulent eddies may be just right.

Numerical calculation

Details of the numerical calculation are as follows. The FLUENT code used in the present study uses the finite volume method for the discretization of all the governing equations (see, for example, Ferziger and Peric[19]). This method involves formal integration of the governing equations of the fluid flow over each of the control volumes of the solution domain and the substitution of a variety of finite-difference type approximations for the terms in the integrated flow equations representing processes such as diffusion, convection, and sources. This procedure converts the integral equations into a system of algebraic equations. The discretization adopted in the present study is formally second-order accurate. The evaluation of pressure in incompressible flow

Table 2. Fluid and Particle Properties Used in the Present Simulations

Material	Properties
Water	ρ = 998.2 kg/m^3, μ = 0.001003 kg/m s
Sand (quartz)	ρ = 2500 kg/m^3
$CaSO_4$	ρ = 2960 kg/m^3
CaO	ρ = 3320 kg/m^3

requires special treatment. A number of methods are available; the one that is used in the present study is based on the SIMPLE (Semi-Implicit Method for Pressure-Linked Equations) formulation involving a pressure correction equation.[19] This allows the sequential and iterative solution of the discretized and linearized algebraic equations. The iterative solution should be carried out until the residual factors, which indicate by how much the governing equations are not satisfied at the discrete level, are sufficiently low. In the present case, this is done until the residual factors are below 0.00001 for each variable. Comparison of the predicted flow field with the experimental results of Ng et al.[20] obtained using Laser-Doppler Anemometry (LDA) for the case of a six-bladed Rushton turbine rotating in a baffled vessel at a speed of 2165 rpm showed good agreement.

Results and Discussion

Geometry and details of the simulations

The specific values of the various parameters of the geometry chosen in this work correspond to experimental conditions of Raghava Rao et al.,[3] which are listed in Table 1. The mixing system consists of a baffled vessel of diameter of 0.57 m and a height of 0.57 m with the impeller configuration given in Table 1. In the simulations, the bottom wall and the curved

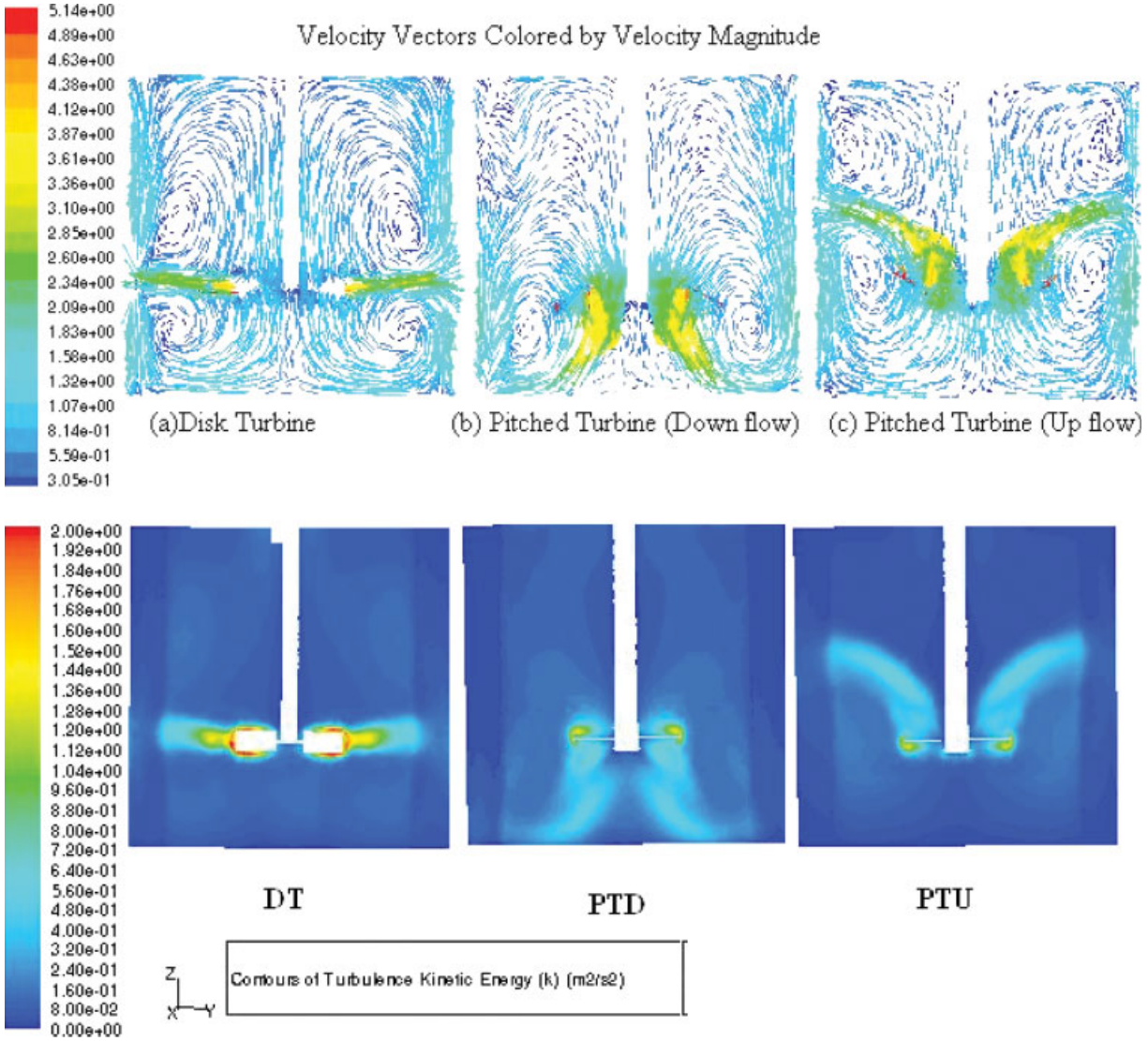

Figure 2. Predicted (a) velocity and (b) turbulent kinetic energy in the vertical plane for a (i) disk turbine, (ii) down flow pitched blade turbine, and (iii) up flow pitched blade turbine at a rotational speed of 500 rpm and for a *T/D* of 3; the impeller tip speed in all cases is 4.97 m/s.

[Color figure can be viewed in the online issue, which is available at www.interscience.wiley.com.]

wall are treated as no-slip boundaries; the top surface, which is the free surface of the liquid, as a flat, shear free boundary. The reference fluid was water and the reference solid particle was sand. A limited number of calculations were also done for other solid properties. These are summarized in Table 2. The study has been conducted using water as fluid in the mixer and various particles are used for one case to study the effect of particle density. The simulations were done with a unstructured grid with grid size of $0.0025 \times T$, giving a total number of cells in the range of 500,000–800,000 depending on the type and diameter of impeller. A large numbers of iterations were required to achieve a converged solution.

Flow field

The computed velocity field for the reference case at an impeller rotational speed of 500 rpm with a *T*/*D* ratio 3 is shown in Figure 2a where the velocity vectors are shown in a vertical plane at the mid section of the tank for the DT, PTD, and PTU. The general flow pattern, characterized by a radial discharge for DT and the mixed radial–axial discharge for the pitched blades (PTD and PTU), is in agreement with the literature. The interaction of the discharge jet with the surrounding tank walls produces a characteristic flow pattern: a double-loop structure in the vertical plane for the DT and the PTU, and a single-loop structure for the PTD. (It should be remembered that the mean flow is not axisymmetric but three-dimensional though periodic.) The overall induced flow field is thus quite distinct in each case although there appears to be a relatively stagnant region at the center of the bottom surface in all the three cases.

The turbulence in the liquid phase plays an important role in the dispersion of the solids. The computed turbulent kinetic energy for the three cases (they all have the identical tip speed of 4.97 m/s) is shown in Figure 2b in the same plane at the same impeller speed. Unlike the secondary flow, which appears to envelope the entire tank, significant levels of turbulence are present only near the impellers. The DT creates high levels of turbulence near the tip of the impeller blade; however, it is dissipated very quickly so that high levels of turbulence are confined only to the impeller plane. The mixed radial–axial discharge of high speed flow for the PTD and PTU gives rise to better distribution of turbulence. As far as the particle dispersion is concerned, the turbulent kinetic energy level near the bottom of the vessel is important. Comparison of the radial profiles of the predicted turbulent kinetic energy below the impeller shows that the PTD, which has its discharge directed towards the bottom wall, has a significantly higher level of turbulent kinetic energy at this height than the other two. PTU, which has its discharge directed away from the bottom wall has the lowest level of turbulence near the bottom. As expected, for the same tank diameter, impeller type and impeller speed, the turbulence intensity increases as the impeller diameter increases. With increasing speed of rotation, the turbulence intensity increases and it appears to scale as $k \sim V_{tip}^2$.

Particle motion and criterion for critical impeller speed

The particle response to the flow field is investigated by tracking the particle of given size and density injected from a point near the top. The trajectories of four sand particles of sizes of 600, 750, 1050, and 1200 μm in the flow field set up by a DT of *T*/*D* ratio of 3 rotating at 500 rpm are shown in Figure 3. Particles of different sizes follow to different degrees the fluid motion; the smallest of the four, namely, the 600-μm particle is well-entrained by the fluid motion; the 750-μm particle to a less extent, whereas the 1200-μm particle is more or less unaffected by the fluid motion except in the plane of the impeller where the velocities are the maximum. Particles of intermediate sizes, namely, 750 μm (Figure 3b), and 1050 μm (Figure 3c) spend significant amounts of time near the bottom of the tank before being entrained. To get a more quantitative picture of this, the variation with time of the normal distance from the tank bottom is plotted in Figure 4 for particles of sizes of 650, 850, and 1050 μm. The 650-μm particle (Figure 4a) approaches the bottom several times but is immediately entrained so that it is not stationary at the bottom for any stretch of time. The 850-μm particle (Figure 4b) spends several seconds (of the

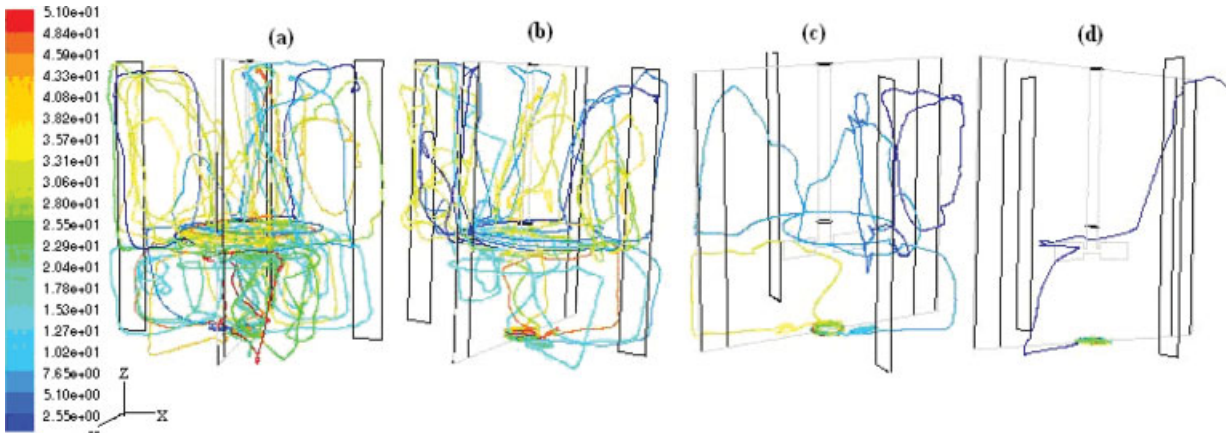

Figure 3. Predicted trajectories of sand particles in water with a disk turbine of *T*/*D* of 3 rotating at 500 rpm: Case of a (a) completely suspended particle (600 μm), (b) critically suspended particle (750 μm), (c) completely settled particle after some time (1050 μm), and a (d) completely settled particle (1200 μm).

[Color figure can be viewed in the online issue, which is available at www.interscience.wiley.com.]

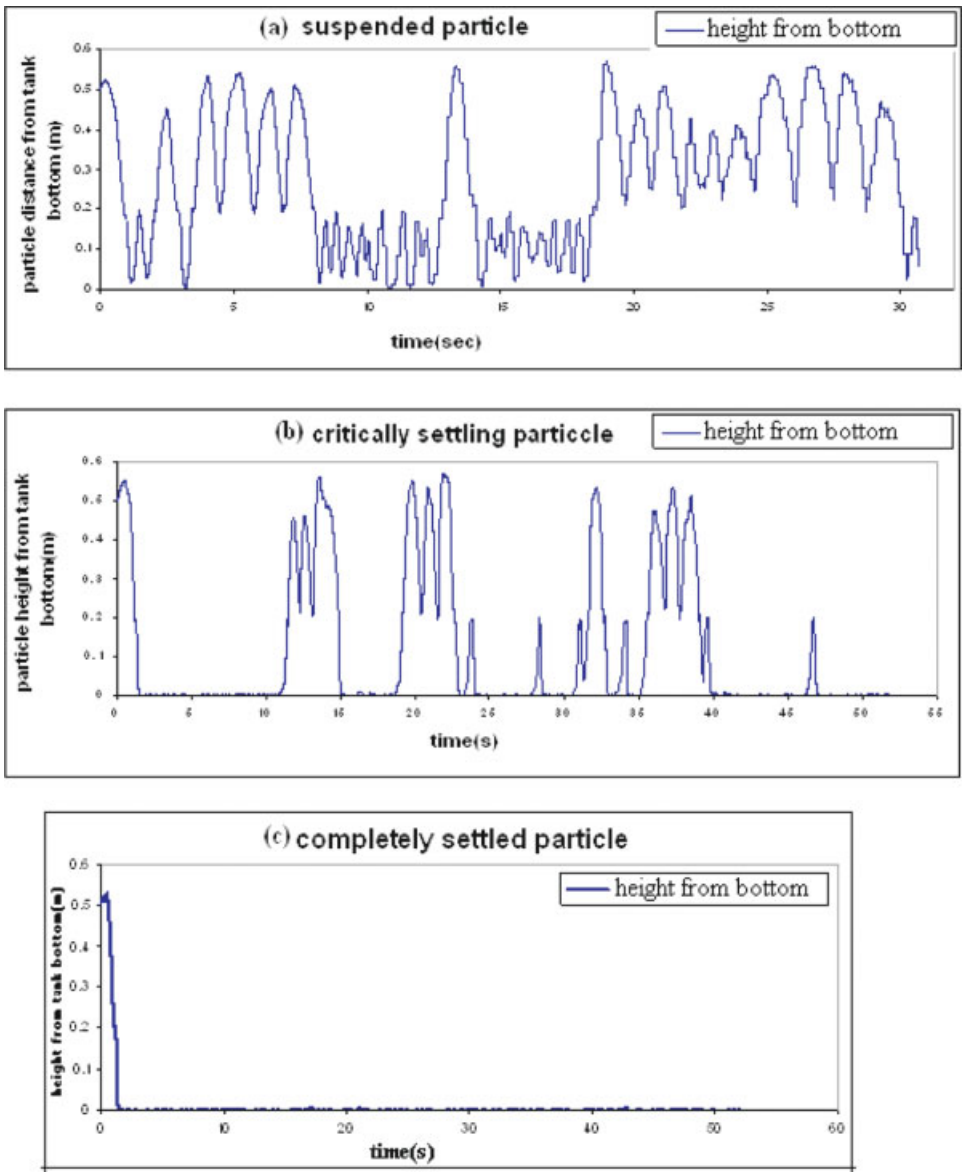

Figure 4. Variation of the normal distance from the bottom wall of particle with time for a disk turbine of *T/D* of 3 rotating at 500 rpm for particle sizes of (a) 650, (b) 850, and (c) 1050 μm.

[Color figure can be viewed in the online issue, which is available at www.interscience.wiley.com.]

order of 3–5 s) at a time before it is entrained, whereas the 1050-μm particle is unable to move from the bottom once it reaches there. Clearly, Figure 4 does not give the complete picture of the particle motion, but it clearly demarcates—in a way similar to that done experimentally—a size range of particles, which can be termed to be critically suspended. For the conditions (geometry of the tank-impeller-fluid-particle system and the rotational speed of the impeller) shown in Figures 3 and 4, this may be taken as ~800 μm. In a CFD simulation, it is easy to calculate trajectories for different particles at the same speed than to compute for the trajectories for the same particle at different speeds (as one would do in an experiment). Thus, while one would get from the experiment the critical speed at which a given particle is critically suspended for a given fluid-vessel-impeller system, one could get from CFD simulations, using a similar criterion (that a critically suspended particle does not spend more than 1–5 s at the bottom at a time[21]), the size of a critically suspended particle for a given fluid-tank-impeller system for a given impeller speed.

Factors affecting size of the critically-suspended particle

To see if the critical suspension of the particle is sensitive, in the expected way, to the parameters of simulations, further calculations have been done, in which the effect of the impeller speed, the role of turbulence, and the density and sphericity of the particle have been investigated, and the results obtained have been summarized in Figure 5. Figure 5a shows the effect of increasing particle density in the form of calculated critical particles for particles of sand, calcium sulphate, and calcium oxide having densities, respectively, of

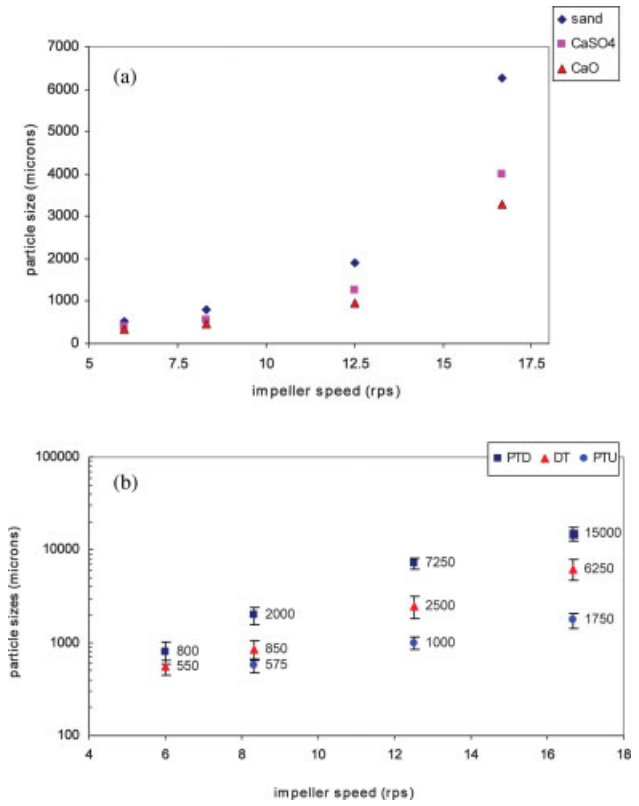

Figure 5. Effect of (a) particle density and (b) impeller type on the critical particle size for a disk turbine of *T/D* of 3.

[Color figure can be viewed in the online issue, which is available at www.interscience.wiley.com.]

2500, 2960, and 3320 kg/m^3 at various impeller speeds. As the particle density increases, its terminal velocity increases and a higher fluid velocity is required to keep it suspended. If the fluid velocity is kept unchanged (because the impeller speed remains the same), then the critical particle size should decrease. This effect is clearly seen in Figure 5a. The influence of turbulent dispersion depends on magnitude of the root mean square (rms) turbulence intensity relative to the particle terminal velocity. If the rms value of turbulence intensity is small compared with the terminal velocity, then there is very little effect of turbulent dispersion on the critical suspension. Similarly, if the rms value of the turbulent intensity is higher than the particle terminal velocity, then turbulence in the liquid will not allow the particle to settle. Similarly, the sphericity of the particle has an important effect on the critical suspension size. Comparative calculations have been done for sphericity factors of 1.0, 0.85, and 0.70 for the DT with a *T/D* ratio of 3. The lower the sphericity factor, the higher is its drag coefficient[22] and therefore the lower will be its terminal velocity. This will have the effect of increasing the critical particle size for a given rotational speed. The effect is higher at high Reynolds numbers because the role of turbulent dispersion becomes more predominant.

As shown in Figure 2, different impellers of identical overall geometrical parameters produce different flow fields. The comparison of different types of impellers with regard to their ability to suspend a sand particle is shown in Figure 5b. Here, the critical particle size for a given rotational speed is bounded by two limits: a lower limit corresponding to the size of a largest completely suspended particle, and an upper limit corresponding to the size the smallest completely settled particle. This gives an idea of the possible subjectivity in the determination of the critical particle size. It is noted that this range is fairly small compared with the particle size. The estimated critical particle sizes for DT, PTD and PTU impellers is shown over the impeller speed range of 360–1000 rpm for a sand-water system with an assumed sphericity of unity. It can be seen that the size of the particle that can be suspended by PTD impeller is much larger than what is possible with DT and PTU impellers. This can be attributed to the turbulence field generated by the impellers. As shown in Figure 2b, the turbulence level predicted for the PTD is much higher than for the other two impellers. While the turbulence generation is nearly the same for PTU and PTD, the turbulent jet is directed away from the bottom in the case of PTU whereas it is in the right position with the PTD, as far as critical suspension—based on the criterion that the particles do not spend more than a few seconds at the bottom of the vessel—is concerned. The role of turbulent dispersion in particle suspension is evident again from the fact that the difference in the suspension abilities of the impellers becomes more predominant at high impeller speeds.

Comparison with experimental data

The predictions of the critical suspension velocity can be compared with experimental data to see how quantitatively good the predictions are. To this end, the experimental data of Rewatkar et al.[4] have been used. They conducted critical suspension experiments with a water and sand system, using PTD, PTU, and DT impellers. While they studied the effect of gas sparging and particle concentration, their data at zero gas velocity and particle concentration of 0.34% (which satisfies the dilute suspension assumption made in the present study) only have been used here for comparison. In the experiments, the speed of the impeller is varied for a fixed particle size, and whereas in the simulations the particle size is varied for a fixed impeller speed (as the particle trajectories of several sizes can be calculated readily with the same continuous phase flow field). The results of the comparison are shown in Figure 6. The agreement is fairly good for all the three impellers in the range of parameters investigated.

Discussion and Conclusion

The present CFD simulations of sand particle suspension in water in stirred vessels using an Eulerian/Lagrangian approach shows that a criterion similar to that used in experimental studies can be established to determine the critical suspension of particles in a CFD simulation. The predicted effect of the principal parameters, namely, the size and density of the particle and the impeller dimensions on the critical impeller speed is in good agreement qualitatively with experimental data from the literature. Studies with different impeller systems having distinct flow patterns shows that the

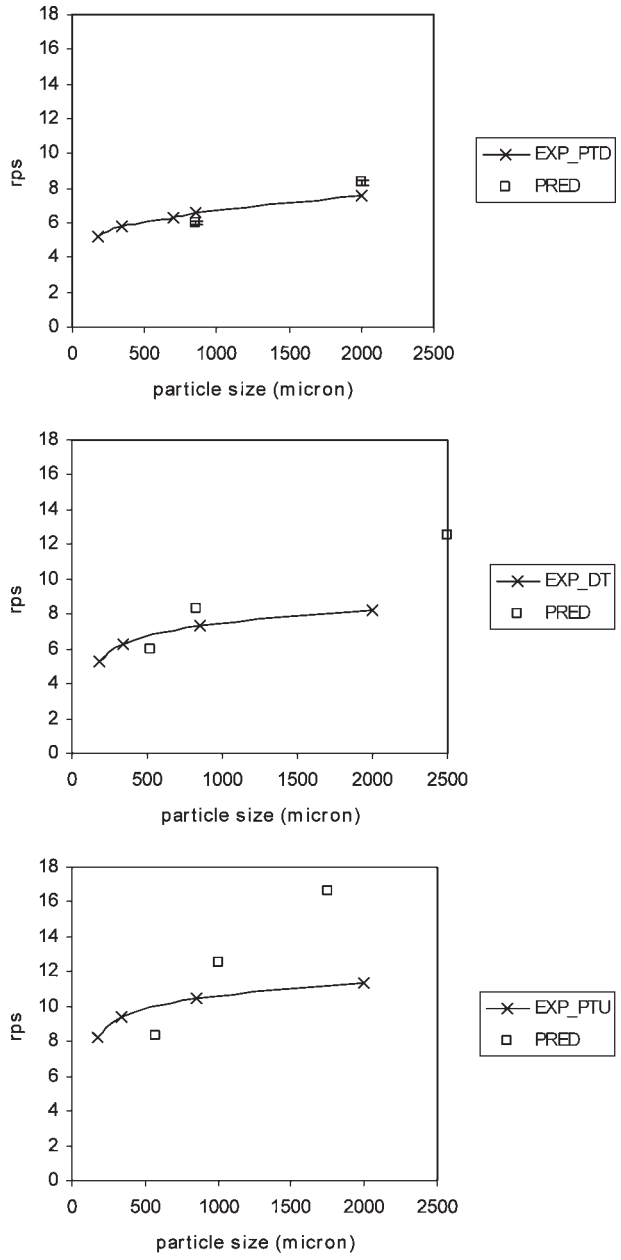

Figure 6. Comparison between the predicted and the experimental data of Rewatkar et al. of critical suspension of sand particles.

linkage between the hydrodynamics within the stirred tank system and the particle suspension is correctly captured. This paves the way for a mechanistic prediction of the effect of nonideal effects, such as irregular geometry, internal parts, multiple impellers, etc., on the critical speed.

While it has been possible to demonstrate qualitative agreement with experimental data for various parameters, careful calibration of the predictions is necessary to obtain quantitative predictions. One of the uncertainties with the present approach (which also exists for the Eulerian/Eulerian approach) is the drag coefficient of the particle. For spherical particles, well-established correlations are available. If the particle shape is significantly different from that of a sphere, a systematic deviation is possible. A second limitation of this approach is treatment of turbulent dispersion of particles. The model used in the present study takes account, for a large number of particle trajectory calculations, of only the energy containing eddies. While this may be sufficient to determine the condition of critical suspension of particles, the dispersion of smaller particles by smaller eddies is not considered; hence the degree of well-mixedness of suspended particles cannot be accurately modeled. Finally, the approach is limited only to dilute suspensions. However, calculations carried out using estimated density and viscosity of the solid–liquid slurries of particle loadings of up to 30% by weight reflect the experimentally-observed trend that the critical suspension speed increases as the particle loading increases.

The results obtained in the present study demonstrate that particle suspension in stirred tanks can be analyzed from first principles using CFD simulations of the type described here. Such studies can be used to optimize the geometry and operating parameters under actual conditions thereby eliminating uncertainties associated with neglecting the effect of internal parts or those arising from scaling up from laboratory-scale studies.

Literature Cited

1. Zweitering TN. Suspending of solid particles in liquid by agitators. *Chem Eng Sci*. 1958;8:244–253.
2. Nienow AW. Suspension of solid particles in turbine agitated baffled vessels. *Chem Eng Sci*. 1968;23:1453–1459.
3. Raghava Rao KSMS, Rewatkar VB, Joshi JB. Critical impeller speed for solid suspension in mechanically agitated solid-liquid contactors. *AIChE J*. 1988;34:1332–1340.
4. Rewatkar VB, Raghava Rao KSMS, Joshi JB. Critical impeller speed for solid suspension in mechanically agitated three-phase reactors. I. Experimental part. *Ind Eng Chem Res*. 1991;30:1770–1784.
5. Armenante PM, Nagamine EU, Susanto J. Determination of correlations to predict the minimum agitation speed for complete solid suspension in agitated vessels. *Can J Chem Eng*. 1978;76:413–419.
6. Murugesan T. Critical impeller speed for solid suspension in mechanically agitated contactors. *J Chem Eng Jpn*. 2001;34:423–429.
7. Nagata S. *Mixing: Principles and Applications*. Tokyo, Japan: Wiley, 1975.
8. Harnby N, Edwards MF, Nienow AW. *Mixing in the Process Industries*. London, UK: Butterworths, 1985.
9. Tatterson GB. *Scale-Up and Design of Industrial Mixing Processes*. New York, USA: McGraw-Hill, 1994.
10. Micale G, Montante G, Grisafi F, Brucato A, Godfrey J. CFD simulation of particle distribution in stirred vessels. *Trans Inst Chem Eng A*. 2000;78:435–444.
11. Micale G, Montante G, Magelli F, Brucato A, Godfrey J. Experiments and CFD predictions of solid particle distribution in a vessel agitated with four pitched blade turbines. *Trans Inst Chem Eng A*. 2001;79:1005–1010.
12. Sha Z, Palosaari S, Oinas P, Ogawa K. CFD simulation of solid suspension in a stirred tank. *J Chem Eng Jpn*. 2001;34:621–626.
13. Barrue H, Bertrand J, Cristol B, Xuereb C. Eulerian simulation of dense solid-liquid suspension in multi-stage stirred vessel. *J Chem Eng Jpn*. 2001;34:585–594.
14. Kee CS, Tan RBH. CFD simulation of solids suspension in mixing vessels. *Can J Chem Eng*. 2002;80:1–6.
15. Derksen JJ. Numerical simulation of solids suspension in stirred tank. *AIChE J*. 2003;49:2700–2714.
16. Shekhar SM, Jayanti S. Mixing of pseudo-plastic fluids using helical ribbon impellers. *AIChE J*. 2003;49:2768–2772.

17. Tanguy PA, Lacroix R, Bertrand F, Chopling L, Brito de la Fuente E. Finite element analysis of viscous mixing with a helical ribbon-screw impeller. *AIChE J*. 1992;38:939–944.
18. Hutchinson P, Hewitt GF, Dukler AE. Deposition of liquid or solid dispersions from turbulent gas streams: a stochastic model. *Chem Eng Sci*. 1971;26:419–439.
19. Ferziger JH, Peric M. *Computational Methods for Fluid Dynamics*. New York, USA: Springer, 1999.
20. Ng K, Fentiman NJ, Lee KC, Yianneskis M. Assessment of sliding mesh CFD predictions and LDA measurements of the flow in a tank stirred by a Rushton impeller. *Trans Inst Chem Eng A*. 1998;76: 737–747.
21. Chudacek MW. Relationships between solid suspension criteria, mechanism of suspension, tank geometry, and scale up parameters in stirred tanks. *Ind Eng Chem Fundam*. 1986;25:391–401.
22. Yow HN, Pitt MJ, Salman AD. Drag correlations for particles of regular shape. *Adv Powder Technol*. 2005;16:363–372.

Manuscript received May 27, 2007.